Quantum-classical correspondence of strongly chaotic many-body spin models

Luis Benet,[1] Fausto Borgonovi,[2,3] Felix M. Izrailev,[4,5] and Lea F. Santos[6]

[1]*Instituto de Ciencias Físicas, Universidad Nacional Autónoma de México (UNAM), Av. Universidad s/n, Col. Chamilpa, CP 62210 Cuernavaca, Mor., Mexico*

[2]*Dipartimento di Matematica e Fisica and Interdisciplinary Laboratories for Advanced Materials Physics, Università Cattolica, via della Garzetta 48, 25133 Brescia, Italy*

[3]*Istituto Nazionale di Fisica Nucleare, Sezione di Milano, via Celoria 16, I-20133 Milano, Italy*

[4]*Instituto de Física, Benemérita Universidad Autónoma de Puebla, Apartado Postal J-48, Puebla 72570, Mexico*

[5]*Dept. of Physics and Astronomy, Michigan State University, E. Lansing, Michigan 48824-1321, USA*

[6]*Department of Physics, University of Connecticut, Storrs, 06269 Connecticut, USA*

(Received 9 December 2022; revised 26 March 2023; accepted 14 April 2023; published 26 April 2023)

We study the quantum-classical correspondence for systems with interacting spin particles that are strongly chaotic in the classical limit. This is done in the presence of constants of motion associated with the fixed angular momenta of individual spins. Our analysis of the Lyapunov spectra reveals that the largest Lyapunov exponent agrees with the Lyapunov exponent that determines the local instability of each individual spin moving under the influence of all other spins. Within this picture, we introduce a rigorous and simple test of ergodicity for the spin motion, and use it to identify when classical chaos is both strong and global in phase space. In the quantum domain, our analysis of the Hamiltonian matrix in a proper representation allows us to obtain the conditions for the onset of quantum chaos as a function of the model parameters. From the comparison between the quantum and classical domains, we demonstrate that quantum quantities, such as the local density of states (LDoS) and the shape of the chaotic eigenfunctions written in the noninteracting many-body basis, have well-defined classical counterparts. We also find a relationship between the Kolmogorov-Sinai entropy and the width of the LDoS, which is useful for studies of many-body dynamics.

DOI: 10.1103/PhysRevB.107.155143

I. INTRODUCTION

The quantum-classical correspondence (QCC) principle is one of the deepest concepts of physics and has attracted significant attention since the birth of quantum physics. The different nature between classical and quantum mechanics is at the origin of the QCC problem; this difference being highly pronounced in deterministic Hamiltonian systems. One of the first rigorous results connecting quantum and classical physics that is often mentioned in the current literature is the Ehrenfest theorem [1]. It states that narrow quantum packets propagate along the classical trajectories for a finite timescale t_E during which the spread of the packets in the phase space can be neglected.

Until the birth of the theory of quantum chaos, the Ehrenfest theorem served as the main tool for establishing the QCC. However, the application of this theorem to quantum systems that exhibit chaotic motion in the classical limit led to unexpected results. As analytically shown in [2], when the system is classically chaotic, the quantum packets spread exponentially fast resulting in a very short physical timescale t_E on which there is complete correspondence between the quantum and classical descriptions of the deterministic systems' behaviors (see also discussion in [3]).

The estimate of the Ehrenfest time for the simplest one-dimensional chaotic systems is given by the expression $t_E \propto \lambda^{-1} \ln(1/\hbar_{\rm eff})$, which depends on *both* the classical Lyapunov exponent λ and the effective quantum parameter $\hbar_{\rm eff}$ proportional to the Planck constant $\hbar$. This expression reveals two cornerstones in the theory of the QCC. The first one is that the more unstable the classical motion is, the shorter the time t_E becomes. The second is that by moving deeper into the quantum region, the Ehrenfest time t_E shrinks.

The first numerical study of a paradigmatic model of classical and quantum chaos, the kicked rotor [4], revealed another timescale, $t_D \gg t_E$, on which there is a good QCC for the width of the quantum packet as it diffusively spreads in momentum space. The process of quantum diffusion gradually slows down, and for times $t \gg t_D$, a complete saturation takes place, while classical diffusion continues. The semianalytical approach developed in [3,5] showed that the saturation results from the localization of the eigenstates that are involved in the dynamics. Due to the finite size of the eigenstates in the infinite momentum space, only a fraction of the phase space can be covered by the quantum packet. Measuring the localization length l_∞ of the eigenstates by projecting them onto the unperturbed basis in which the dynamics is explored, it was found numerically and explained semianalytically that l_∞ is proportional to the classical diffusion coefficient D_{cl}. This direct link between classical diffusion and the localization of the eigenstates is an important finding in the theory of quantum chaos. It became known as dynamical localization and is observed in various disordered models.

As a result of the discovery of the two timescales on which the chaotic properties of motion get manifested in a quantum system, t_E and t_D, the question arose about when the

correspondence principle holds. Local properties of chaos are evident in quantum systems on timescales $t \lesssim t_E$, while for global properties, this happens for $t < t_D$. This means that in quantum systems, manifestations of chaos depend on the time at which the evolution of the system is considered. Thus, we have to agree that there is no unique answer to the validity of the correspondence principle itself. The answer does not depend only on the generally accepted classical limit $\hbar_{\rm eff} \to 0$, but also on how the limit is taken, whether before or after the time limit $t \to \infty$. If, for example, we fix $\hbar_{\rm eff}$ and let time go to infinity first, the correspondence principle will be violated. If, on the other hand, we assume that the correct procedure is to take $\hbar_{\rm eff} \to 0$ first, the course of action becomes to fix a finite time when taking $\hbar_{\rm eff} \to 0$, and only next take $t \to \infty$, therefore "saving" the correspondence principle as applied to chaotic systems. (The question of which limit should be taken first arises also in classical physics when investigating integrable nonlinear systems with a large number N of degrees of freedom, the issue in this case being the order of the limits $N \to \infty$ and $t \to \infty$.)

Taking $\hbar_{\rm eff} \to 0$ first was the solution to the QCC problem proposed by Chirikov at the beginning of the quantum chaos theory [3]. According to Chirikov, chaotic properties are observed in quantum systems at finite times only, be the time short or long. Similar points have been partially addressed in several recent studies [6–25] that relate unstable classical motion with the exponentially fast evolution of quantum observables, including the out-of-time ordered correlator (OTOC) [26]. In these works, the QCC is mostly restricted to short times, typically on the same order as the Ehrenfest time.

Further numerical studies comparing classical and quantum diffusion [27] led to the conclusion that the observed quantum diffusion, although nicely reproducing the global properties of classical diffusion, is not *true* diffusion, because quantum diffusion is reversible in time, in contrast to diffusion in classical physics. By numerically reversing the evolution, the initial quantum packet is completely recovered, while this is not possible in a classical system due to the exponential sensitivity of the chaotic motion to any weak perturbation. In essence, chaos that occurs in quantum systems at times $t > t_E$ for some global observables has a different nature from chaos emerging in classical physics.

There have been several efforts to relate essential properties of a (pseudo)chaotic quantum dynamics to the statistical properties of spectra and eigenstates. One of the earliest suggestions in this direction was Berry's conjecture that for quantum billiards fully chaotic in the classical limit, the eigenstates may be treated as random superpositions of plane waves [28]. In this sense, quantum chaos can be understood as the complicated (random) structure of the stationary states in a physically chosen basis (see also [29–34]). As for the eigenvalues, the properties of the energy spectra of quantum systems that are strongly chaotic in the classical limit should be comparable to those determined by random matrices of a specific symmetry [35,36].

The interest in the statistical properties of the energy spectra of complex quantum systems emerged before the birth of quantum chaos. It was motivated by experimental studies of heavy nuclei and many-electron atoms (see, e.g., [37,38] and references therein). One of the first questions addressed was the shape of the distribution $P(s)$ of the spacings s between nearest energy levels in relation to the results from experiments with nucleon scattering on nuclei. It was observed that the probability of small spacings decreases with s, thus manifesting repulsion between nearest-neighboring energy levels. After intensive discussions about the form of $P(s)$, Wigner suggested the expression that is nowadays known as the Wigner surmise [39], obtained with the use of simple scaling arguments. Later, he indicated that the form of $P(s)$ could be explained within the theory of random matrices. Further studies of random matrices (see the collection of papers in [40]) showed that the degree of repulsion for small spacings s depends on the symmetry of the random matrices or, equivalently, on the underlying symmetry of the physical systems. Although there is no analytical expression valid for any value of s, it was numerically shown [41] that an exact form written as an infinite sum is quite close to the approximate expression given by the Wigner surmise.

The relationship between the properties of the energy spectra of quantum systems that are strongly chaotic in the classical limit and the spectra of random matrices emerged in studies of billiards [35,36] and was supported with semiclassical analysis [42]. In the other limit of completely integrable classical systems, it was understood [43] that the form of $P(s)$ can be approximately described by the Poisson distribution $P(s) \sim \exp(-s)$. This distribution was analyzed within a semiclassical approach to quantum systems in [28]. The Berry-Tabor conjecture [28] of the Poisson form of $P(s)$ is considered a generic property of integrable quantum systems with a classical limit, but despite intensive mathematical studies (see [44–46] and references therein), it has not yet been rigorously proved. Recent studies [47] of the Lieb-Liniger quantum model, known to be integrable and solvable with the Bethe ansatz [48,49], have shown that the Berry-Tabor conjecture fails due to the existence of underlying correlations between energy levels. Other papers that have discussed the onset of level repulsion in integrable systems include Refs. [50–54].

As one moves from few- to many-body systems, the analysis of the correspondence principle gets more challenging [18,19,55–61]. With regard to classical systems, this is primarily due to the structure of the multidimensional phase space, which becomes practically inaccessible for a detailed study. On the quantum side, the main problem is the dimension of the Hilbert space, which grows exponentially fast with the number of particles and sites. As a result, many questions about the QCC applied to many-body systems remain unanswered.

The purpose of this paper is to resolve the issue of the QCC for many-body systems, at least partially, by focusing on the strongly chaotic regime. Our study is based on the semianalytical approach that was used to establish the criteria for the onset of quantum chaos and statistical relaxation in isolated quantum systems of interacting Fermi and Bose particles, and which were confirmed by numerical experiments [34,62–64].

We consider a one-dimensional spin model that is relevant to experiments with ion traps, where the range of the interactions can be tuned [65–68]. We show that quantities used

in the analysis of quantum dynamics, quantum chaos, and localization have classical counterparts. The QCC between these quantities becomes excellent in the region of quantum chaos. We also find a direct relationship between the rate of quantum information spread and the Kolmogorov-Sinai entropy, which is a classical quantity obtained by summing the positive Lyapunov exponents.

The paper is organized as follows. In Sec. II, we describe our one-dimensional classical system with L interacting spins and determine the range of parameters chosen for our numerical simulations. As we explain, the analysis of the system's behavior in the multidimensional phase space is simplified due to additional integrals of motion. The phase space of the system represents a set of L three-dimensional (3D) spheres, each one corresponding to one spin. The motion of each spin is limited by a 3D phase space and is described by a 3D equation with an external perturbation determined by the behavior of the surrounding spins. As a result, the degree of instability of the motion of a single spin is effectively determined by the positive Lyapunov exponent associated only with that individual spin and not with the entire system of spins. This allows us to relate the maximal Lyapunov exponent of each single spin with the Kolmogorov-Sinai entropy of the whole system. In addition, we are able to obtain a rigorous and simple definition of ergodicity for the entire classical system by examining the motion of each spin on its 3D sphere.

Section III describes the corresponding quantum system and gives an estimate of the critical interaction strength above which the behavior of the quantum system can be considered chaotic. The estimate is done before diagonalization and is based on the structure of the Hamiltonian matrix represented in a properly chosen noninteracting basis. Numerical analysis of level statistics supports the analytical estimates that we obtain.

In Sec. IV we show that it is possible to define classical analogues to functions that are widely used in the analysis of quantum systems. One of these functions is known in nuclear physics as strength function and in solid state physics as local density of states (LDoS). The other refers to the shape of the eigenfunctions (SoE) and is used to quantify the eigenstates as either localized or delocalized, and as regular or chaotic. The LDoS and the SoE for classical systems are obtained by numerically integrating the classical equations of motion [69,70]. The possibility to talk about the classical LDoS and the classical SoE remains little known, despite some previous studies [71–75]. Our numerical data demonstrate an excellent correspondence between the classical and quantum functions above the quantum chaos border. The knowledge of these functions is extremely important for the description of the dynamical properties of the quantum system and its relaxation into a state that can be described statistically [34].

Inspired by the QCC, several results have been obtained relating the behavior of quantum observables—such as survival probability, Loschmidt echo, different types of entropies, and OTOCs—with the maximal Lyapunov exponent in the region of strong chaos [7,10,11,13,17,22,25,76]. However, many-body classical systems are characterized by the full spectrum of Lyapunov exponents and many features of global dynamics can be thought in terms of the sum of all positive Lyapunov exponents [77], that is, the Kolmogorov-Sinai entropy. This prompts us to search for a link between quantum dynamics and the Kolmogorov-Sinai entropy, a direction taken also in [78–80]. It was recently shown that the width of the quantum LDoS determines the dynamical wave packet spreading in the noninteracting many-body Hilbert space [64,81] and is related with the timescale for equilibration. In Sec. V, we then compare the width of the LDoS with the Kolmogorov-Sinai entropy and find a direct correspondence between the two. Conclusions are given in Sec. VI.

II. CLASSICAL MODEL

We consider a one-dimensional classical model of L interacting spins described by the following Hamiltonian:

$$H = H_0 + V = \sum_{k=1}^{L} B_k S_k^z - \sum_{k=1}^{L-1} \sum_{j>k}^{L} J_{jk} S_j^x S_k^x, \tag{1}$$

where

$$B_k \equiv (B_0 + \delta B_k),$$

and

$$J_{jk} \equiv \frac{J_0}{|j-k|^\nu}.$$

The angular momentum $I^2 = |\vec{S}_k|^2$, for $k = 1, \ldots, L$, is fixed. We choose $I = 1$, so that time has the dimension of inverse energy. In Eq. (1), B_k are the frequencies of the noninteracting motion described by the Hamiltonian H_0. They are slightly detuned by random values of δB_k, with $|\delta B_k| \leqslant \delta W \ll B_0$, to avoid degeneracies in the corresponding quantum model. We consider a single set of random values of δB_k, so the model is perfectly deterministic, in the sense that no averages over different realizations of Hamiltonians are performed. The interacting part of the Hamiltonian depends on the couplings J_{jk} between all pairs of spins and decays algebraically with the distance between the spins with an exponent $\nu > 1$. Even though there is coupling between distant spins, technically speaking, since the model is one-dimensional and $\nu > 1$, we are not considering long-range interactions. Most of our results are obtained for the generic value of $\nu = 1.4$ and do not depend on this choice.

The classical equations of motion are obtained from standard expressions written in terms of the Poisson brackets and the Levi-Civita symbol $\epsilon^{\alpha\beta\gamma}$ as

$$\left\{S_k^\alpha, S_j^\beta\right\} = \delta_{kj} \epsilon^{\alpha\beta\gamma} S_k^\gamma, \tag{2}$$

from which we have

$$\begin{aligned} \dot{S}_k^x &= \left\{S_k^x, H_0\right\} = -B_k S_k^y, \\ \dot{S}_k^y &= \left\{S_k^y, H\right\} = B_k S_k^x + S_k^z \sum_{j\neq k} J_{jk} S_j^x, \\ \dot{S}_k^z &= \left\{S_k^z, V\right\} = -S_k^y \sum_{j\neq k} J_{jk} S_j^x. \end{aligned} \tag{3}$$

The numerical solution of the classical dynamics is obtained by integrating, via the 9/8 Runge-Kutta algorithm,

the equations of motion in Eq. (3). To make the comparison between quantum and classical dynamics as close as possible, the initial conditions for the classical system are chosen using random directions for the spins in the Bloch sphere under either the constraint of (i) fixed noninteracting energy in a sufficiently small microcanonical energy range $E_0 - \delta E_0 < H_0 < E_0 + \delta E_0$, or of (ii) fixed total energy $E - \delta E < H < E + \delta E$. For each result, we specify whether condition (i) or (ii) is used.

When analyzing the structure of the phase space of model (1), it is important to take into account that in addition to the total energy, there are L other integrals of motion, namely the squares of the angular momenta of each spin, which are fixed. In other words, the classical trajectory of each individual spin lies on a sphere of unit radius, which is separated from the other spins. The influence of the surrounding spins to the stability of an individual spin can be regarded as an external perturbation. From this viewpoint, the equation for the k-th spin can be written as

$$\ddot{S}_k^z + \Omega_k^2(t) S_k^z = F_k(t), \tag{4}$$

with the nonlinear time-dependent frequency

$$\Omega_k^2(t) = \left[\sum_{j\neq k} J_{jk} S_j^x(t)\right]^2 = J_0^2 \left[\sum_{j\neq k} \frac{S_j^x(t)}{|j-k|^\nu}\right]^2, \tag{5}$$

and the driving nonlinear force

$$\begin{aligned} F_k(t) &= \sum_{j\neq k} J_{jk}\left[B_j S_j^y(t) S_k^y(t) - B_k S_j^x(t) S_k^x(t)\right] \\ &= J_0 \sum_{j\neq k} \frac{B_j S_j^y(t) S_k^y(t) - B_k S_j^x(t) S_k^x(t)}{|j-k|^\nu}. \end{aligned} \tag{6}$$

Equation (4) indicates that the z component of each single spin can be thought of as a parametric oscillator with a time-dependent frequency $\Omega_k(t)$ and under the force $F_k(t)$ that depends on the sum of the product of all x and y spin components.

The picture above implies that, in addition to the stability of the motion of the total system consisting of L oscillators (spins), one can ask about the stability of any individual spin. Notice that the motion of a single spin is itself nonlinear, but for weak interactions between spins, the nonlinear terms can be treated perturbatively. This representation of our model helps to understand the essential properties of the motion. Specifically, in the weak interaction limit, the motion of the S^z component of a chosen oscillator can be considered separately from the S^x and S^y components.

A somewhat similar model of parametric oscillators was analyzed by Chirikov in his seminal paper [82,83], in which he discovered that the overlaps of nonlinear resonances result in the phenomenon of chaotic motion. These resonances appear in the second order of perturbation theory, which complicates the analytical approach. The rigorous analysis of such *nearly-linear* models of interacting particles, where the nonlinearity is due to the perturbative coupling with other degrees of freedom, is still an open problem (see [84]).

In the following two subsections we study the properties of our system with the purpose of identifying, if any, the region of maximal classical chaos. We also give a physical insight of what maximal chaos actually means.

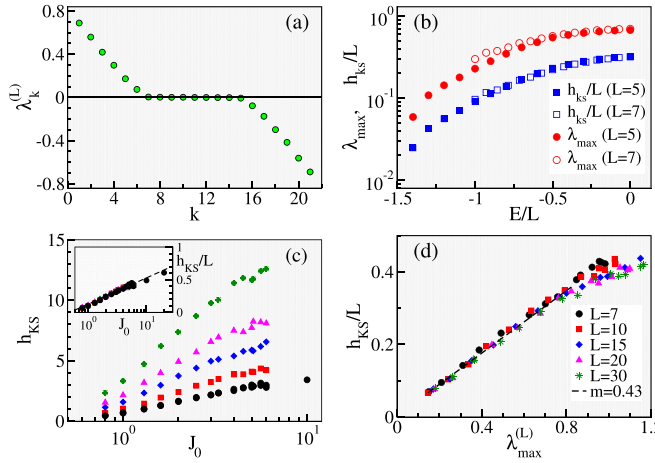

FIG. 1. (a) Lyapunov spectrum for $L = 7$ spins showing L positive, L negative, and L null exponents. (b) Average (over initial conditions) of the maximal Lyapunov exponent and average density of the Kolmogorov-Sinai entropy as a function of the energy per spin E/L for two different system sizes L. (c) Average Kolmogorov-Sinai entropy as a function of J_0 (in semilog scale) for different values of L [see legend in (d)]. (Inset) Rescaled Kolmogorov-Sinai entropy as a function of J_0 showing the collapse into a single curve. (d) Average Kolmogorov-Sinai entropy density vs average maximal Lyapunov exponent for different values of L; same values of J_0 as in (c). Dashed line is the best linear fit (m is the slope) for all data in the region $\lambda_{\max}^{(L)} < 0.8$. Deviations from the linear dependence appear for $\lambda_{\max}^{(L)} > 0.8$, since this region is characterized by large values of the interaction strength, $J_0 \gg B_0$. In all panels: $B_0 = 1$, $\delta W = 0.2$, and $\nu = 1.4$. In (a),(b): $J_0 = 3$. In (b): Average over an ensemble of 300 initial random trajectories within a small energy window ± 0.01 around the indicated energy values in the x axis. In (c),(d): Fixed energy $|E| < 0.01$ and the average is done over 10^3 initial values of $S^{x,y,z}$.

A. Lyapunov analysis

To study the chaotic properties of the classical many-body system, we perform the standard Lyapunov analysis, which consists in finding the Lyapunov spectrum $\lambda_1, \lambda_2, \ldots \lambda_{3L}$ [85]. We compute the whole Lyapunov spectrum by integrating the variational equations together with the equations of motion [86,87]. This is done by choosing random initial conditions at a fixed energy E. Since the length of each spin is a constant of motion, L exponents are equal to zero. In addition, due to the time-reversal symmetry, the eigenvalues satisfy $\lambda_k = -\lambda_{3L-k}$, for $k = 1, ..L$, hence there are only L positive Lyapunov exponents. The spectrum is illustrated in Fig. 1(a) for $L = 7$. Notice that the Lyapunov exponents corresponding to $k = 7$ and $k = 15$ are very close to zero, but are not zero.

From the Lyapunov spectrum, we obtain the Kolmogorov-Sinai entropy $h_{\rm KS}$ which is defined via the Pesin theorem [88] as the sum of all positive Lyapunov exponents,

$$h_{\rm KS} = \sum_{k=1}^{L} \lambda_k^+. \tag{7}$$

Our main interest is in the maximal Lyapunov exponent $\lambda_{\max}$. For two sufficiently close initial conditions on the constant energy surface, the distance between the two trajectories in the multidimensional phase space grows exponentially in time with a rate given by $\lambda_{\max}$. Its inverse $1/\lambda_{\max}$ defines the shortest timescale related to the dynamical instability.

In what follows, we use the results in Fig. 1 to describe the direct relationship between the maximal Lyapunov exponent and the Kolmogorov-Sinai entropy. In particular, Fig. 1(b) shows that both quantities are similar functions of energy and Fig. 1(d) demonstrates that $h_{\rm KS}/L \propto \lambda_{\max}$.

Generically, the Lyapunov exponents and the Kolmogorov-Sinai entropy depend on the initial conditions, such as the energy or the particular regions of the energy surface, and on the chosen parameters L, B_0, J_0, and the range of the interaction ν. To show this dependence, we fix $B_0 = 1$, which sets the energy scale, keep $\nu = 1.4$, choose a sufficiently large interaction strength $J_0 = 3$, and study in Fig. 1(b) $\lambda_{\max}$ and $h_{\rm KS}$ as a function of the energy of the initial conditions. Here and hereafter, the notation for the maximal Lyapunov exponent $\lambda_{\max}$ and for the Kolmogorov-Sinai entropy $h_{\rm KS}$ indicate the average values obtained within an ensemble of random initial conditions with constant energy E. As seen in Fig. 1(b), both the maximal Lyapunov exponent and the Kolmogorov-Sinai entropy are smooth increasing functions of the energy density E/L. We therefore choose $E = 0$ as the region of maximal dynamical instability (chaos) for our further investigations. In the numerical simulations $E = 0$ means $-0.01 < E < 0.01$.

It is important to note that fixing the value of the energy does not fix the degree of chaos, since we still have the freedom to tune the interaction strength J_0. This is actually a subtle point that deserves better clarifications. Contrary to the common intuition, increasing the interspin interaction strength J_0 while keeping the energy fixed at $E = 0$ does not increase the contribution of the interacting part V in comparison with the noninteracting part H_0. Fixing the initial conditions to have $E = 0$ means that $|H_0| \simeq |V|$, so for any J_0, both H_0 and V remain on the same order of magnitude. Physically, changing the strength of the perturbation J_0 while keeping the energy E fixed just means exploring different regions of the energy surface $E = 0$. That is, increasing J_0 corresponds to selecting a set of initial conditions where, on average, the modulus of the z magnetization, $|(1/L)\sum_k S_k^z|$, also increases. This is a generic feature found whenever one fixes the total energy rather than changing the ratio between the interacting part (V) and the noninteracting part (H_0) of the Hamiltonian.

Figure 1(c) shows that the Kolmogorov-Sinai entropy grows logarithmically with respect to the interaction strength J_0, even for small $J_0 < 1$. To better understand the dependence of $h_{\rm KS}$ on the system size L, we plot in the inset the density of the Kolmogorov-Sinai entropy $h_{\rm KS}/L$ as a function of J_0. As one can see, the data obtained for different values of L collapse into a single curve, showing that the rescaling with respect to the system size is excellent. These results should be compared with those contained in [85], where an analogous rescaling was found for the discrete nonlinear Schrödinger chain.

For values of J_0 that are not too large with respect to B_0, the (average) maximal Lyapunov exponent shows a dependence on the interaction strength similar to that of the density of Kolmogorov-Sinai entropy. To facilitate the comparison, we plot one quantity as a function of the other in Fig. 1(d). There is a linear relation between them, $h_{\rm KS}/L = m\lambda_{\max}$, where $m \simeq 0.43$ is the slope obtained by the best linear fitting for not too large values of $\lambda_{\max}$. This relationship is in agreement with the approximate linear dependence of the positive part of the Lyapunov spectrum as a function of k seen in Fig. 1(a).

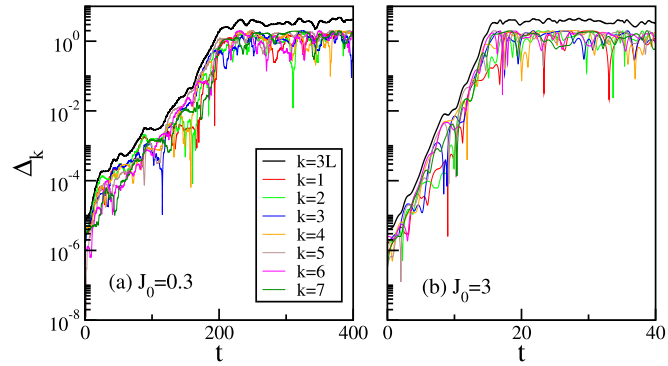

FIG. 2. Distance between two close trajectories in time. Black thick line is the Euclidean distance in the $3L$ dimensional space, while coloured lines stand for the distance in the 3D space for different spin numbers $k = 1, .., L$, where $L = 7$. The parameters are $\alpha = 1.4$, $B_0 = 1$, $\delta W = 0.2$, initial energy $E = 0 \pm 0.01$, and interaction strength $J_0 = 0.3$ (a) (weak chaos) and $J_0 = 3$ (b) (strong chaos). Only one trajectory is considered.

Concerning the physical meaning of these results, let us first point out that the dependence of both $h_{\rm KS}$ and $\lambda_{\max}$ on $\ln J_0$, as evident from Figs. 1(c) and 1(d), raises the question of the contribution of each spin to the growth in time of the phase space volume. Indeed, since a coarse-grained volume $\mathcal{V}$ in the phase space is expected to grow exponentially in time with an exponent given by $h_{\rm KS}$ [77,89], we should have

$$\mathcal{V}(t) = \mathcal{V}(0)\, e^{h_{\rm KS} t} \propto \left[J_0^L\right]^t. \tag{8}$$

The equation above indicates that even in the presence of a strong inter-spin interaction, each spin contributes individually to the growth of this volume. This behavior must be related with the presence of the L constants of motion, being therefore generic for spin systems. It would be interesting to test this result in other classical spin chains.

Another important point that we raise, motivated by the equations of motion [Eq. (4)] for the single spins, is the relationship between the maximal Lyapunov exponent of the multidimensional problem and the dynamical instability of the trajectory of each individual spin confined to its 3D sphere. To address this question, we compare the dynamics of the Euclidean distance between two initially close trajectories for each spin k, $\Delta_k(t) = ||\vec{S}_k(t) - \vec{S}'_k(t)||$, with the Euclidean distance for the many-dimensional problem, $\Delta_{3L} = [\sum_{k=1}^{L} ||\vec{S}_k(t) - \vec{S}'_k(t)||^2]^{1/2}$. The results are shown in Fig. 2 for two values of the interaction strength J_0. Despite fluctuations, one sees that the exponential growth of $\Delta_k(t)$ for each spin k coincides with the maximal Lyapunov exponent of the many-body spectrum. This means that the timescale for the dynamical instability on each individual Bloch sphere

is also described by the maximal Lyapunov exponent of the multidimensional problem, a result that is far from trivial.

B. Ergodicity of the classical motion

The finding above that the motion of each spin is characterized by the maximal positive Lyapunov exponent means that the motion is *locally* strongly chaotic. However, this does not imply that global properties, such as the relaxation of the whole system of L spins, follow the predictions of statistical mechanics. For this reason, we now investigate whether our system exhibits ergodicity. Apart from simple specific systems, such as billiards and two-dimensional maps, a mathematical proof of ergodicity for interacting many-body systems is still missing. The usual numerical approach is to search for consequences of ergodicity, such as the decay of correlations functions, which is still not enough to claim ergodicity.

Here, we introduce a very simple and rigorous way to study the onset of ergodicity. Since the motion of each spin is confined to its 3D sphere, a rigorous definition of ergodicity means that the distribution of each one of the three Cartesian components of each single spin should follow the expression for each component of the random eigenstates of N-dimensional full random matrices [90,91],

$$P(S) = \frac{\Gamma(N/2)}{\sqrt{\pi}\Gamma((N-1)/2)}(1-S^2)^{(N-3)/2} \tag{9}$$

where $\Gamma(N)$ is the Gamma function. In the case of $N \to \infty$, this expression leads to the Gaussian distribution of the eigenvectors components. Since in our case we have $N = 3$, the ergodic distribution implies the constant result $P(S) = 1/2$. This method significantly simplifies the study of ergodicity for spin models.

To test ergodicity in our system, we consider a single initial condition $u(0) = \{\vec{S}_1(0), .., \vec{S}_L(0)\}$ at a fixed energy $E = 0$ and compute the trajectory $u(t)$ under the full Hamiltonian H for a very long time, $T = 10^5$. We then build the distribution obtained by sampling each component $S^k_\alpha(t_j)$, where $\alpha = x, y, z$ and $k = 1, .., L$, at different times $t_j = j/T$, $j = 1, .., T$. The interval $[-1, 1]$ in which each single spin component can vary is divided in 10^2 bins and we count the number of times each single spin component visits each single bin. We say that the motion is ergodic when the distribution $P(S^k_\alpha) = 1/2$ within the statistical error.

The results for the distributions $P(S^x)$, $P(S^y)$, and $P(S^z)$ for various interaction strengths J_0 are shown in Figs. 3 and 4 for $L = 6$ and $L = 60$, respectively. Each color represents a different spin number $k = 1, \ldots, L$.

In Figs. 3(a)–3(c), where chaos is weak, the distribution of S^z is clearly different from that of the components S^x and S^y. This can be understood from the equations of motion, Eq. (4). In the absence of interaction, the motion of each spin is simply a rotation about the z axis. In the presence of weak interaction strength J_0, these oscillators get coupled, resulting in a motion that covers ergodically a portion of the surface of the 3D sphere. For even larger J_0, the motion eventually covers the whole surface. Looking at Fig. 3, as J_0 increases to $J_0 = 1$ [Figs. 3(d)–3(f)] and $J_0 = 3$ [Figs. 3(g)–3(i)], $P(S^z)$ becomes more similar to $P(S^x)$ and $P(S^y)$, but the distributions do not get flat, so the motion cannot be considered truly ergodic for this system size ($L = 6$), even when the interaction strength is large (by significantly increasing J_0, the distributions become even more curved).

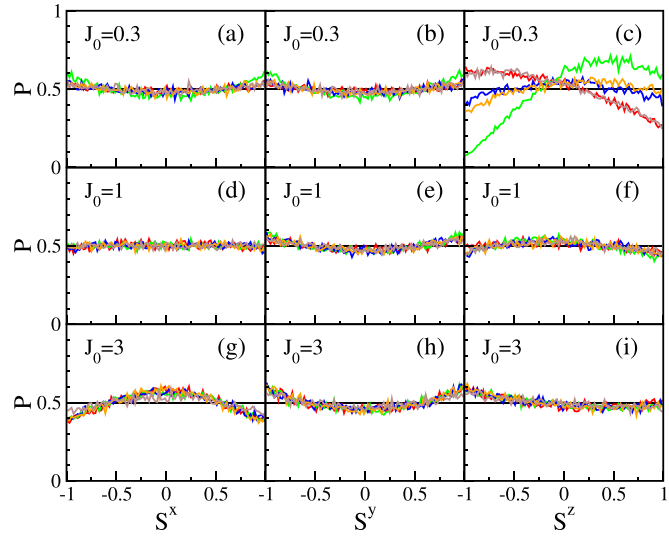

FIG. 3. Probability distribution functions $P(S^x)$ [(a),(d),(g)]; $P(S^y)$ [(b),(e),(h)], and $P(S^z)$ [(c),(f),(i)] for $J_0 = 0.3$ [(a)–(c)], $J_0 = 1$ [(d)–(f)], and $J_0 = 3$ [(g)–(i)]. Solid horizontal black line indicates the theoretical result for ergodicity, $P(S_k^{x,y,z}) = 1/2$. Parameters: $L = 6$, $B_0 = 1$, $\nu = 1.4$, $\delta W = 0.2$. Initial conditions: random spins with energy $E = 0$. Integration time $T = 10^5$. Only one trajectory is considered.

By increasing the system size L, our data in Fig. 4 show a clear onset of ergodicity provided the interaction strength is

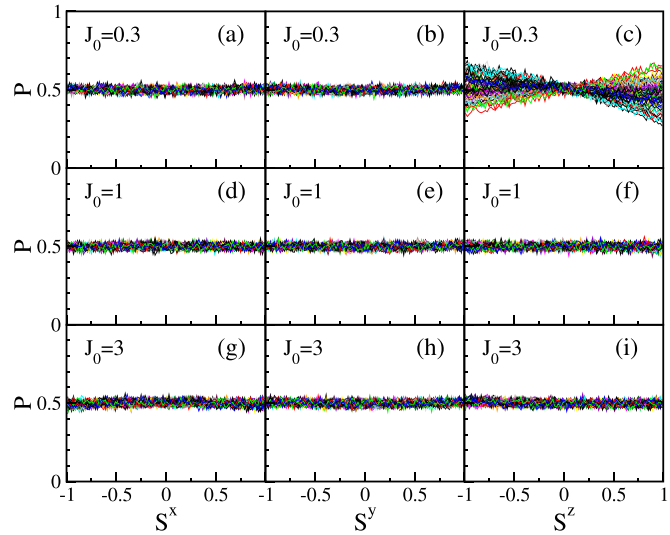

FIG. 4. Probability distribution functions $P(S^x)$ [(a),(d),(g)]; $P(S^y)$ [(b),(e),(h)], and $P(S^z)$ [(c),(f),(i)] for $J_0 = 0.3$ [(a)–(c)], $J_0 = 1$ [(d)–(f)], and $J_0 = 3$ [(g)–(i)]. Solid horizontal black line (clearly visible in Fig. 3) indicates the theoretical result for ergodicity, $P(S_k^{x,y,z}) = 1/2$. Parameters: $L = 60$, $B_0 = 1$, $\nu = 1.4$, $\delta W = 0.2$. Initial conditions: random spins with energy $E = 0$. Integration time $T = 10^5$.

strong enough, $J_0 \gtrsim 1$. Therefore, ergodicity for the motion of any single spin requires a large number of spins. A possible reason for the lack of ergodicity for $L = 6$ is the presence of stability islands due to nonlinearity. This has been observed for $L = 2$ in Ref. [71] and references therein.

We reiterate that to have strong statistical properties one should have *both* strong chaos, signalled by a positive maximal Lyapunov exponent, and ergodicity.

III. QUANTUM MODEL

Upon quantization we have, for each spin,

$$|\vec{S}^2| = \hbar^2 S(S+1) = 1,$$

where S is the quantum spin number and the z component of the spin has the values $\hbar s$ with $s = -S, -S+1 \ldots, S-1, S$. For simplicity, we only consider integer spin numbers S. Here, and below $\hbar = 1/\sqrt{S(S+1)}$ plays the role of an effective Planck constant. In other words, the classical limit is obtained for large spin numbers $S \gg 1$.

We build the many-body Hilbert space of the total quantum Hamiltonian,

$$\hat{H} = \hat{H}_0 + \hat{V}, \tag{10}$$

using the z representation, where the basis $|n\rangle$ corresponds to the many-body eigenstates of the noninteracting Hamiltonian $\hat{H}_0$ and have noninteracting energies $E_n^{(0)}$,

$$\hat{H}_0|n\rangle = \sum_{k=1}^{L} (B_0 + \delta B_k)\hat{S}_k^z|n\rangle \equiv E_n^{(0)}|n\rangle, \tag{11}$$

with

$$|n\rangle = |s_1, \ldots, s_k, \ldots, s_L\rangle,$$

and

$$\hat{S}_k^z|n\rangle = \hat{S}_k^z|s_1, \ldots, s_k, \ldots, s_L\rangle = \hbar s_k|s_1, \ldots, s_k, \ldots, s_L\rangle.$$

The interacting part of the classical Hamiltonian (1) is written in terms of operators as

$$\hat{V} = \sum_{j>k}^{L} \sum_{k=1}^{L-1} \frac{J_0}{|j-k|^\nu} \hat{S}_j^x \hat{S}_k^x. \tag{12}$$

The interparticle interaction is computed by taking into account that $\hat{S}_j^x = (\hat{S}_j^+ + \hat{S}_j^-)/2$ and

$$\hat{S}_k^\pm|s_1, \ldots, s_k, \ldots, s_L\rangle = \hbar\sqrt{S(S+1) - s_k(s_k \pm 1)}|s_1, \ldots, s_k \pm 1, \ldots, s_L\rangle. \tag{13}$$

The two-body interaction in Eq. (12) can be written as $\hat{V} = \hat{V}_{\rm in} + \hat{V}_{\rm out}$, where

$$\hat{V}_{\rm in} = \sum_{j \neq k} \frac{J_0}{4|j-k|^\nu} (\hat{S}_j^+ \hat{S}_k^- + \hat{S}_j^- \hat{S}_k^+) \tag{14}$$

and

$$\hat{V}_{\rm out} = \sum_{j \neq k} \frac{J_0}{4|j-k|^\nu} (\hat{S}_j^+ \hat{S}_k^+ + \hat{S}_j^- \hat{S}_k^-). \tag{15}$$

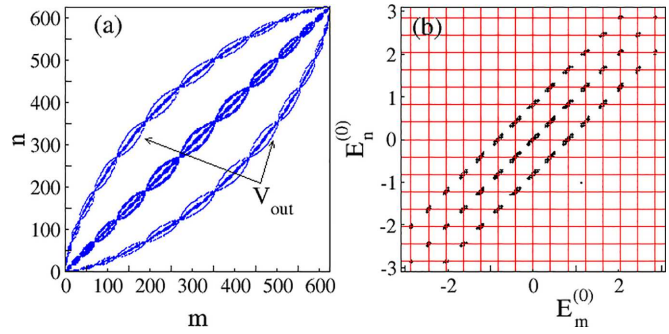

FIG. 5. Structure of the full Hamiltonian in the site representation (a) and in the energy representation (b). The block diagonal structure is evident. In (b), the red vertical and horizontal lines indicate multiples of $\hbar B_0$. For both panels: $B_0 = 1$, $\delta W = 0.04$, $J_0 = 3$, $\nu = 1.4$, $L = 4$, $S = 2$.

The term $\hat{V}_{\rm in}$ couples spin configurations that have the same total magnetization along the z axis, $\hat{M}_z = \sum_{k=1}^{L} \hat{S}_k^z$, so it does not change the value of the quantum number $\mu_z = -LS, -LS+1, \ldots, LS-1, LS$. The term $\hat{V}_{\rm out}$ couples basis vectors that differ by two excitations, so it changes the total magnetization by a factor of two, $\mu_z \to \mu_z \pm 2$. The eigenvalues can then be divided as belonging to an even (in units of $\hbar$) or odd value of the total z-magnetization. The model is not integrable for any choice of the parameters $J_0 \neq 0$, $B_0 \neq 0$, $\nu \neq 0$.

A. Hamiltonian matrix structure and quantum chaos border

Information about the structure of the Hamiltonian matrix is fundamental for a complete description of the system in terms of quantum chaos [34]. From the structure of the matrix, one can estimate the quantum chaos border, that is, the interaction strength necessary to produce chaotic eigenstates and thus relaxation and eventually thermalization [34,92]. The full analysis of the Hamiltonian matrix, eigenvalues, and eigenstates provides a more complete picture than relying only on the statistics of the spacings between neighboring energy levels.

We order the many-body noninteracting states from low to high energies and analyze the structure of the Hamiltonian matrix in two representations. The site representation is used in Fig. 5(a), where the label n in the axis indicates a many-body noninteracting state $|n\rangle$ and each colored dot marks a nonzero element $\langle n|\hat{H}|m\rangle \neq 0$. In Fig. 5(b), each dot indicates again an element $\langle n|\hat{H}|m\rangle \neq 0$, but the labels in the x and y axes are now the noninteracting energies $E_n^{(0)}$. This noninteracting energy representation is more physical and it allows for generalizations to other many-body models.

To provide a detailed analysis of the Hamiltonian matrix, let us discuss first its noninteracting part $\hat{H}_0$, which commutes with $\hat{M}_z$. This means that in the many-body S_z representation the H_0 matrix has a block-diagonal structure with $2SL+1$ blocks, each block being associated with a quantum number μ_z. The block structure is indeed observed for the diagonal elements in Figs. 5(a) and 5(b).

All levels belonging to a single block would be degenerate if $\delta B_k = 0$. Instead, we have random $|\delta B_k| \leqslant \delta W \ll B_0$, so

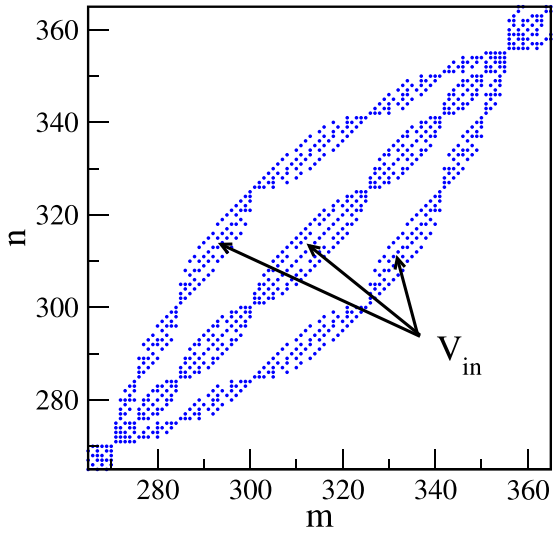

FIG. 6. Structure of the central block ($\mu_z = 0$) of the Hamiltonian $\hat{H}_0 + \hat{V}_{\rm in}$ in the site representation. $B_0 = 1$, $\delta W = 0.04$, $J_0 = 3$, $\nu = 1.4$, $L = 4$, $S = 2$.

each block of noninteracting levels forms an energy band whose maximal width is estimated to be $\approx 2L\delta W$. This can be confirmed by considering the central block with $\mu_z = 0$ (which is the largest block) and a generic state $|n_0\rangle = |s_1, \ldots, s_L\rangle$ belonging to it. The noninteracting energy of this state is given by

$$\langle n_0|\hat{H}_0|n_0\rangle = \hbar \sum_k s_k \delta B_k,$$

which is maximized for $s_k = S$ and $\delta B_k = \delta W$, so that $E^{(0)}_{\rm max} = \hbar SL\delta W$, $E^{(0)}_{\rm min} = -\hbar SL\delta W$, and the energy size of the central block can be estimated as

$$\Delta_0 = E^{(0)}_{\rm max} - E^{(0)}_{\rm min} \simeq 2\hbar SL\delta W \simeq 2L\delta W. \qquad (16)$$

Since the energy distance between the diagonal blocks is proportional to $\hbar B_0$ [see the horizontal and vertical red lines in Fig. 5(b)], when $B_0 > 2LS\delta W$, the diagonal elements are arranged in $2LS + 1$ disconnected segments, as indeed seen in Figs. 5(a) and 5(b), while for $B_0 \lesssim 2LS\delta W$, all elements along the diagonal become more or less homogeneously distributed.

We now move to the interacting part of the Hamiltonian, starting with the term $\hat{V}_{\rm in}$ in Eq. (14) that only couples states inside the same block of fixed μ_z value, since it commutes with $\hat{M}_z$. Let us then concentrate on a single block with fixed μ_z. In Fig. 6(a), we show the central block ($\mu_z = 0$) and the arrows indicate examples of nonzero elements caused by the interactions within that block, $\langle n|\hat{V}_{\rm in}|m\rangle \neq 0$.

The two-body interaction $\hat{V}_{\rm in}$, which contains the sum of the operators $\hat{S}^+_j \hat{S}^-_k$, exchanges the state of two spins that at most have a noninteracting energy difference $\delta\epsilon = \hbar|B_k - B_j| \simeq 2\hbar\delta W \simeq 2\delta W/S$.

The term $\hat{V}_{\rm out}$ in Eq. (15) couples the elements of one block with those of a next-nearest-neighboring block, and as such, it allows us to compute the entire width of the Hamiltonian matrix. The arrows in Fig. 5(a) indicate examples of nonzero elements caused by the interactions between the central block and outer blocks, $\langle n|\hat{V}_{\rm out}|m\rangle \neq 0$. To estimate the energy bandwidth of the total Hamiltonian matrix, we sum the energy separation between the two outer bands connected with the $\mu_z = 0$ central band, that is $\approx 4\hbar B_0$ with the width of the outer band $2L\delta W$: $\Delta E \simeq 4B_0/S + 2L\delta W$.

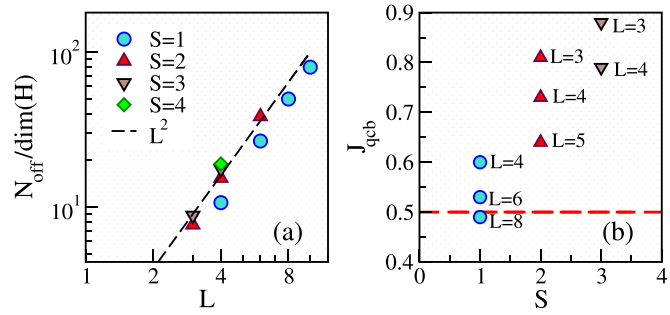

FIG. 7. (a) Number of off-diagonal matrix elements $N_{\rm off}$ rescaled by the dimension of the many-body Hilbert space $\dim(H) = (2S + 1)^L$ as a function of the system size L for different values of S. The dashed line is $\propto L^2$. (b) Interaction strength for the quantum chaos border J_{qcb} as a function of S for different values of L. The dashed line is our estimate for the chaos border. The parameters in both panels are $B_0 = 1$, $\delta W = 0.2$, $J_0 = 1$, $\nu = 1.4$.

In hands of the bandwidth of the Hamiltonian matrix, one now needs the number of directly coupled states, so that dividing that bandwidth by this number, one obtains the many-body energy spacing. To induce quantum chaos, the interaction strength has to be larger than the energy spacing, i.e., the chaotic regime emerges when the interaction is strong enough to mix all neighboring many-body levels.

The average number of directly coupled states corresponds to the average number of nonzero off-diagonal elements in each row of the Hamiltonian matrix. This number should be proportional to the number of local operators in the interacting part of the Hamiltonian $\hat{V}$, that is $\propto L^2$. Numerically, we compute the total number of off-diagonal matrix elements $N_{\rm off}$ of the full Hamiltonian matrix and divide it by the matrix dimension, $\dim(H) = (2S + 1)^L$. This is done in Fig. 7(a) for different values of L and S, confirming that indeed $N_{\rm off}/\dim(H) \propto L^2$. The quantum chaotic regime appears when the typical perturbation strength (strength of the off-diagonal elements) is able to mix many-body levels, whose energy separation can be estimated by $\Delta E/L^2$. The strength of the perturbation is proportional to J_0, but it also depends in a complicated way on the other parameters ν, L, and S, so we denote the strength of the off-diagonal elements of the matrix Hamiltonian by $J_0|V_{j,k}|$. One can then estimate that strong quantum chaos emerges when

$$J_0 \gtrsim \frac{\Delta E}{L^2|V_{j,k}|} \equiv J_{qcb}, \qquad (17)$$

where J_{qcb} designates the interaction strength for the quantum chaos border (qcb).

In Fig. 7(b), J_{qcb} is shown as a function of S for different system sizes K. As one can see, for the parameters used in the numerical investigations of this paper ($S = 1, 2, 3$, $B_0 = 1$, $\delta W = 0.2$, $\nu = 1.4$, $L = 5, 6, 7$), an "operative" estimate for the quantum chaos border indicates $J_0 \gtrsim 0.5$. However, it is evident that J_{qcb} depends on the length L, as also noticed in

[93–95], and on the spin quantum number S, so it is difficult to make further analytical considerations concerning the chaos border both in the semiclassical and thermodynamic limit. In the next section, we corroborate the consistency of our choice $J_0 \gtrsim 0.5$ by studying level statistics.

In closing this section let us stress that even if each two-body spin Hamiltonian has its particularities, our analysis can be extended to more general Hamiltonians. Instead of our Hamiltonian, we could have a system with additional transverse magnetic fields along the x, y directions that would also couple the nearest-neighbour blocks, $\mu_z \to \mu_z \pm 1$, or it could be a model with only $\hat{V}_{\rm in}$, or other variations. But overall, the results would be very similar, we would still have very sparse banded matrices due to the presence of two-body couplings. We may therefore say that the Hamiltonian structure analyzed in this paper is quite generic for spin systems with two-body interactions.

B. Level statistics

Quantum systems that are chaotic in the classical limit often exhibit correlated eigenvalues as in random matrices [37]. The degree of short-range correlations can be evaluated with the distribution of the spacing s between neighboring unfolded levels. In the case of random matrices belonging to the Gaussian orthogonal ensemble (GOE), the distribution follows the Wigner surmise, $P_{\rm GOE}(s) = (\pi s/2)\exp(-\pi s^2/4)$, while uncorrelated levels result in a distribution close to the Poissonian distribution $P_{\rm P}(s) = \exp(-s)$ [96].

A more complete picture of the spectrum requires also the analysis of the long-range correlations. To measure the rigidity of the spectrum, one resorts to quantities such as the level number variance $\Sigma^2(\ell)$, which is the variance of the number of unfolded eigenvalues in an interval ℓ. For GOE, we have that $\Sigma^2_{\rm GOE}(\ell) = 2[\ln(2\pi\ell) + \gamma + 1 - \pi^2/8]/\pi^2$, where γ is the Euler constant, while for the Poissonian case, the fluctuations are larger and the variance grows linearly with the energy interval, $\Sigma^2_{\rm P}(\ell) = \ell$.

In Fig. 8, we compare the level spacing distributions [Figs. 8(a)–8(c)] and the level number variances [Figs. 8(d)–8(f)] for different values of the interaction strength J_0, growing from left to right, and keeping fixed the other parameters of the Hamiltonian. For all the chosen values of the interaction, the classical system is always chaotic, but deviations from the Wigner-Dyson distribution are seen in Fig. 8(a), because $J_0 = 0.3$ is below the quantum chaos border. Actually, even in the region where good agreement of the level spacing distribution with the Wigner-Dyson distribution is seen [Figs. 8(b) and 8(c)], deviations from the random matrix theory results appear for the more sensitive measures, such as the level number variance in Figs. 8(e) and 8(f) for $\ell > 7$. Even though this observation is important, it is not surprising, because we are comparing the spectrum of a sparse banded matrix, that has correlated elements, with the spectrum of a GOE random matrix.

IV. SHAPE OF EIGENFUNCTIONS AND LOCAL DENSITY OF STATES

In this section, we discuss two basic concepts for the study of quantum chaos and show that they have classical analogues. The first one is the envelope of the exact eigenstates written as a function of the noninteracting energies, which is referred to as the "shape of the eigenstates" (SoE), and the other is the "local density of states" (LDoS). Both quantities have been extensively investigated in view of the definition of chaotic eigenstates [71,74]. Chaotic eigenstates are defined as eigenstates composed of many components in the noninteracting basis that can be treated as completely uncorrelated.

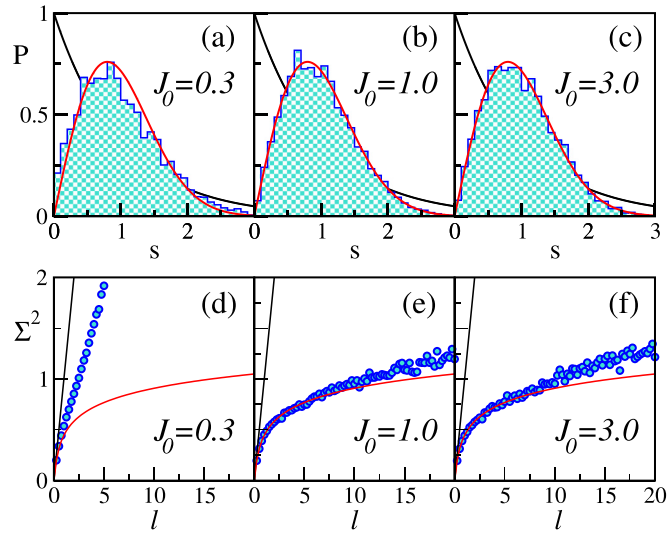

FIG. 8. Nearest-neighbor level spacing distribution [(a)–(c)] and level number variance [(d)–(f)] for three different interaction strengths; $L = 6$, $S = 2$, B_0=1, $\delta W = 0.2$, $\nu = 1.4$. For comparison, the solid lines represent Poisson (black) and GOE (red) results. All the eigenvalues have been computed from one symmetry sector (even total z magnetization) discarding 10% of the levels at the borders.

In physical systems, the eigenstates cannot be fully ergodic in the noninteracting basis due to the finite range of the interactions, which gets reflected in the band-like structure of the total Hamiltonian. Therefore, one can speak at most about pseudorandomness of the eigenstates in connection with some envelope around which the fluctuations of the squared components of the eigenfunction are Gaussian. This envelope can be obtained either by averaging over close eigenstates or by using moving windows within one eigenstate. The equivalence of these two averaging procedures is at the core of statistical mechanics.

Both quantities, SoE and LDoS, are broadly employed in the quantum realm. To fix the notation, the Schrödinger equation

$$\hat{H}_0|n\rangle = E_n^{(0)}|n\rangle \tag{18}$$

defines the noninteracting eigenstates $|n\rangle$ and eigenvalues $E_n^{(0)}$ of $\hat{H}_0$, and

$$\hat{H}|\alpha\rangle = E_\alpha|\alpha\rangle \tag{19}$$

gives the exact eigenstates $|\alpha\rangle$ and exact eigenvalues E_α for $\hat{H}$. We use Latin letters for the noninteracting eigenstates and eigenvalues and Greek for the exact ones. The coefficients

$$C_n^\alpha = \langle n|\alpha\rangle \tag{20}$$

of the eigenfunctions $|\alpha\rangle = \sum_n C_n^\alpha|n\rangle$ written in the noninteracting basis are the building blocks of our approach. They are

obtained from the projection of the exact eigenstates on the noninteracting states or from the projection of the noninteracting states on the exact ones.

A. Shape of the eigenstates

For the quantum SoE, we study the components C_n^α as a function of the noninteracting energies $E_n^{(0)}$. We perform an average $\langle..\rangle$ over the eigenstates in a small energy window, $E-\delta E < E_\alpha < E+\delta E$, and smooth the function,

$$W_E(E^{(0)}) = \sum_n \delta(E^{(0)} - E_n^{(0)}) \left\langle \left| C_n^\alpha \right|^2 \right\rangle. \tag{21}$$

In this equation the SoE $W_E(E_n^{(0)})$ represents the probability that an eigenstate having an energy in the window $[E-\delta E, E+\delta E]$ is found in the noninteracting state of energy $E_n^{(0)}$.

We obtain the classical analog of the SoE by taking random initial conditions for spins with energy fixed in a small window $E-\delta E < H < E+\delta E$ and computing the noninteracting energy $E_n^{(0)} = H_0(\vec{S}_1, \ldots, \vec{S}_L)$ for all of them. From that, the classical probability $w_E(E_n^{(0)})$ to have that particular noninteracting energy (histogram of frequencies) can be obtained.

B. Local density of states

As for the quantum LDoS associated with some noninteracting state $|n\rangle$, a similar procedure is used. The LDoS is obtained from the coefficients C_n^α as a function of the energy of the total Hamiltonian. We perform an average over the noninteracting states in a small energy window, $E^{(0)} - \delta E < E_n^{(0)} < E^{(0)} + \delta E$, and smooth the function,

$$W_{E^{(0)}}(E) = \sum_\alpha \delta(E - E_\alpha) \left\langle \left| C_n^\alpha \right|^2 \right\rangle. \tag{22}$$

This distribution represents the probability for a noninteracting state with energy in the range $[E^{(0)} - \delta E, E^{(0)} + \delta E]$ to be found in the eigenstate with energy E.

Since the quantum LDoS is the energy distribution of a given initial state $|\Psi(0)\rangle$ of the system, it is tightly connected with the system's evolution. The absolute square of the Fourier transform of the LDoS,

$$\int W_{E^{(0)}}(E) e^{-iEt/\hbar} dE = |\langle \Psi(0)|\Psi(t)\rangle|^2,$$

for example, is the survival (return) probability, $|\langle\Psi(0)|\Psi(t)\rangle|^2$, extensively analyzed in studies of quench dynamics (see [34,97–102] and references therein), and the width σ_{LDoS} of the LDoS is associated with the lifetime of the initial state. In fact, in the region of strong chaos, σ_{LDoS} is a key parameter for the description of the relaxation process of quantum systems toward thermalization [64].

To construct the classical LDoS, we fix the noninteracting energy $E^{(0)}$ and take random initial conditions for each single spin on the unit sphere with the noninteracting energy $E^{(0)}$ in the required interval $[E^{(0)} - \delta E, E^{(0)} + \delta E]$. We then compute the total energy E for all of them and obtain the probability $w_{E^{(0)}}(E)$ to have the energy E (histogram of frequencies).

C. Quantum-classical correspondence

The comparison between the classical and quantum SoE and LDoS is done using the components C_n^α of the eigenfunctions and the properties of the classical energy surfaces $H_0 = E_0$ and $H = E$. More precisely, the classical distributions can be thought of as a projection of one of these surfaces onto the other [103,104].

Figures 9(a)–9(c) show a comparison between the quantum SoE (shade) $W_E(E^{(0)})$ and its classical analog (solid line) $w_E(E^{(0)})$. Figures 9(d)–9(f) display the comparison between the quantum LDoS (shade) $W_{E^{(0)}}(E)$, and its classical version (solid line) $w_{E^{(0)}}(E)$. There is excellent quantum-classical agreement above the quantum chaos border, $J_0 > 0.5$, while deviations are seen below the quantum chaos border. To explain the reason for the discrepancy, it is useful to resort to a method to compute the classical SoE and LDoS based on the dynamical equations of motion, as described next.

The procedure to obtain SoE goes as follows. We consider one initial condition specified by the 3L vector $u(0) = \vec{S}_1(0), \ldots, \vec{S}_L(0)$ with energy E in the chosen energy window and consider its evolution $u(t)$ under the full interacting Hamiltonian H. From that we compute the function $E^{(0)}(t) = H_0(u(t)) = H_0(\vec{S}_1(t), \ldots, \vec{S}_L(t))$ at several equally spaced times $t_k = k\Delta t$, where Δt is chosen of the same order of the typical period of the motion $1/B_0$ to have statistical independent data. The function $E^{(0)}(t)$ is shown in Fig. 10(a) and the values at t_k are indicated with circles. The normalized distribution of these points is the SoE shown in Fig. 10(b). It gives the same result as the "static" method used to obtain Fig. 9(a) provided the trajectory can cover ergodically the whole energy range obtained by the phase space sampling. Most importantly, it is only in this situation that we can properly define the classical SoE. In the case in which, due to some physical or dynamical constraints, different trajectories produce different distribution functions, then a proper definition of the classical SoE becomes problematic. We then have the following nontrivial result: *the quantum SoE admits a well-defined classical limit only if the classical motion is ergodic in some energy region.*

This analysis can be equivalently extended to the LDoS, where the dynamical and static methods to compute the classical LDoS give equal results only in the region of strong quantum chaos, and they also coincide with the quantum LDoS. Analogously to SoE, the dynamical construction of the classical LDoS requires a single initial condition $u_0(0) = \vec{S}_1(0), \ldots, \vec{S}_L(0)$ with fixed noninteracting energy $E^{(0)}$ and its evolution $u_0(t)$ under the noninteracting Hamiltonian H_0.

To compute $u_0(t)$ under the noninteracting Hamiltonian we do not need to numerically integrate the equations of motion. The classical evolution under H_0 corresponds simply to rotations of all spins about the z axis with frequencies B_k, and it is given by

$$\begin{aligned}
\left(S_k^x\right)^0(t) &= S_k^x(0)\cos(B_k t) + S_k^y(0)\sin(B_k t),\\
\left(S_k^y\right)^0(t) &= S_k^y(0)\cos(B_k t) - S_k^x(0)\sin(B_k t),\\
\left(S_k^z\right)^0(t) &= S_k^z(0).
\end{aligned} \tag{23}$$

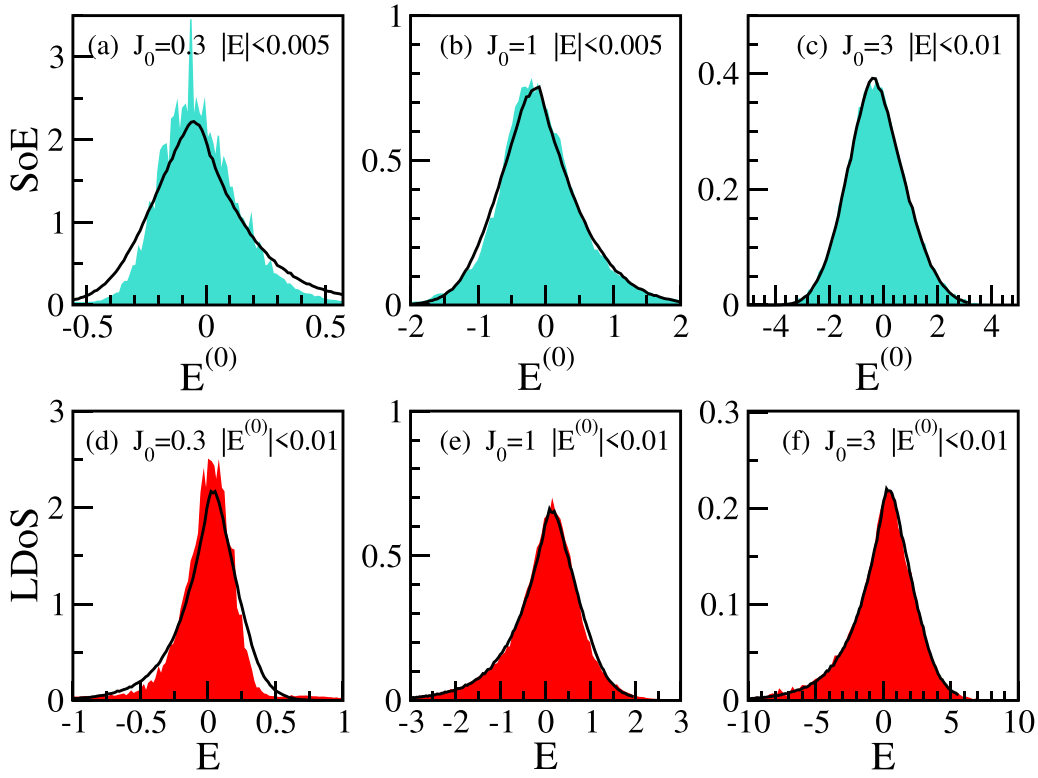

FIG. 9. [(a)–(c)] Quantum (shade) and classical (line) shape of the eigenfunctions. [(d)-(f)] Quantum (shade) and classical (line) local density of states. Parameters: $L = 6$, $B_0 = 1$, $\delta W = 0.2$, $\nu = 1.4$. The quantum-classical correspondence is very accurate for strong enough interaction, $J_0 \gtrsim 1$. For the quantum case, we have $S = 2$ and average over 41 eigenstates for the SoE and 50 noninteracting basis states for the LDoS. For the classical functions, we consider a set of 10^5 initial conditions with total energies (SoE) or noninteracting energies (LDoS) in the same interval of the corresponding quantum model.

With the trajectory under the noninteracting Hamiltonian H_0, we obtain the function $E(t) = H(\vec{S}_1^0(t), \ldots, \vec{S}_L^0(t))$ from where we extract the values at $t_k = k\Delta t$, with $\Delta t \sim 1/B_0$, to build the correspondent normalized histogram.

To understand the mechanism for the discrepancy between the classical and quantum quantities for small interaction strength, $J_0 < 0.5$, as shown in Figs. 9(a) and 9(d), we take the case of the SoE as an example. Needless to say a similar analysis can be done for the LDoS. In Fig. 11 we compare the quantum SoE (shaded area) with the classical SoE

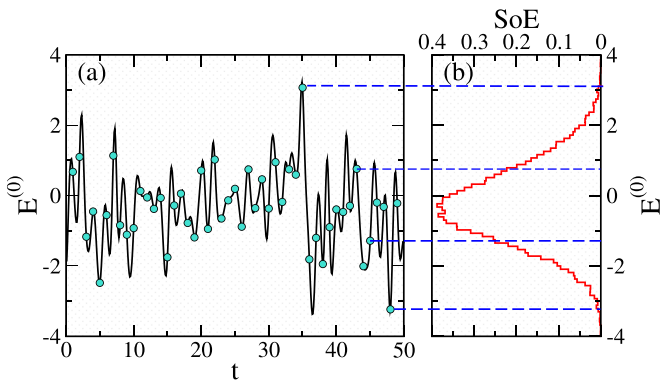

FIG. 10. Dynamical construction of the classical shape of the eigenfunctions. In (a): Trajectory $E^{(0)}(t)$ obtained by inserting in the noninteracting Hamiltonian H_0 the solution of the full equations of motion under the total Hamiltonian H. Random sample of values of $E^{(0)}(t)$ at equally spaced times are represented by circles. In (b): These points, which represent how a trajectory at some specified energy fills the "energy shell" of H_0, are used to plot the normalized probability distribution function.

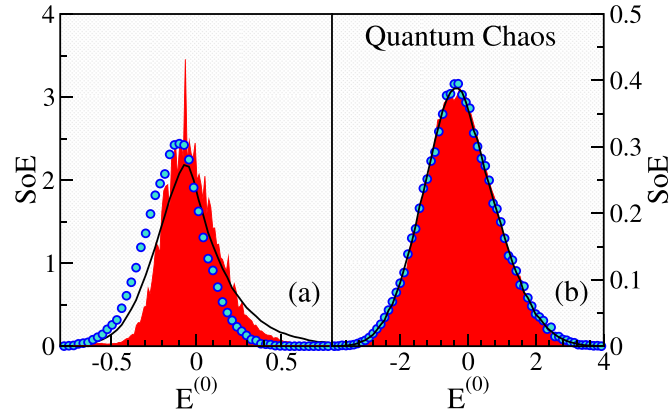

FIG. 11. Classical and quantum shape of the eigenfunctions for two different interaction strengths: $J_0 = 0.3$ (a) and $J_0 = 3$ (b). (Red) histograms represent the quantum data obtained by averaging 41 eigenfunctions in a small energy window in the center of the spectrum. (Black) Full lines stand for the classical SoE obtained by averaging over 10^5 random points in the same small energy window (static method). (Blue) Circles are obtained with a single trajectory with energy $|E| < 0.01$ (dynamical method).

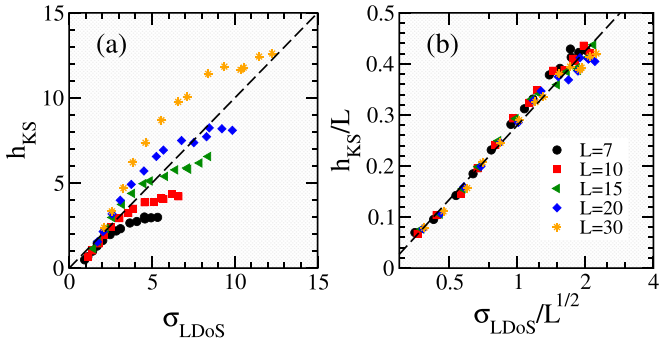

FIG. 12. (a) Comparison between the Kolmogorov-Sinai entropy and the width of the LDoS for $B_0 = 1$, $W = 0.2$, $\nu = 1.4$, initial energy $|E| < 0.01$, and different interaction strengths $0.5 < J_0 < 10$. The dashed line guides the eye and represents the line $y = x$. (b) Comparison between the density of the Kolmogorov-Sinai entropy and the rescaled width of the LDoS for the same data as in panel (a). In the x axis the logarithmic scale has been used. Here, the dashed line stands for the best logarithmic fit $y = 0.28 + 0.21\ln(x)$.

obtained with the static method (line) and with the dynamical method (circles) for two values of the interaction strength. While the three distributions coincide in the quantum chaotic regime [Fig. 11(b)], they differ for small interaction strength [Fig. 11(a)]. The lack of agreement between the two classical distributions in Fig. 11(a) is a clear indication of the lack of ergodicity. Due to dynamical reasons, such as the presence of islands of stability or dynamical constraints, a single trajectory cannot span the whole allowable energy range as defined by the random initial conditions used to implement the static distribution. Surprisingly, even the quantum distribution differs from the classical static one. The fact that the quantum distribution is narrower suggests the presence of quantum localization. This should not to be confused with the lack of classical chaos, since both cases, $J_0 = 0.3$ and $J_0 = 3$, are characterized by the exponential divergence of close trajectories, signalled by a positive maximal Lyapunov exponent.

V. KOLMOGOROV-SINAI ENTROPY AND WIDTH OF THE LDoS

As presented in Fig. 2, the rate of the exponentially growing separation between close trajectories for each individual spin is related with the maximal exponent of the full Lyapunov spectrum of the whole spin system. But what is the role of the other positive Lyapunov exponents? To address this question, we resort to the studies in Zaslavsky's book [77], where he compares the value of the Kolmogorov-Sinai entropy with the exponential growth in time of the coarsed grained phase-space volume for multidimensional classical systems with chaotic behavior, as in our Eq. (8). We have discussed this relation in our previous paper [64] about the onset of quantum chaos in fermionic and bosonic systems characterized by two-body interactions. Specifically, we have argued that the Kolmogorov-Sinai entropy [h_{KS} in Eq. (7)] should be directly related to the width of LDoS [σ_{LDoS} in Eq. (22)]. We now confirm this expectation for our spin system.

Figure 12(a) compares σ_{LDoS} and h_{KS} in the energy range of maximal chaos ($|E| < 0.01$) for different system sizes L and interaction strengths J_0. Different colors indicate different system sizes, and the interaction strength for each set of data grows from the left to the right in the panels. In the chaotic region considered, which is characterized by ergodicity, the classical and quantum LDoS are very close, so one can also see the comparison between the Kolmogorov-Sinai entropy and the width of LDoS in Fig. 12 as a comparison between two well defined, but physically different classical quantities.

In Fig. 12(a), we observe that h_{KS} and σ_{LDoS} are on the same order of magnitude, but deviations are visible, which depend on both the values of L and J_0. In Fig. 12(b), we show the same data, but rescaled as $\tilde{h}_{KS} = h_{KS}/L$ (density of the Kolmogorov-Sinai entropy) and $\tilde{\sigma}_{LDoS} = \sigma_{LDoS}/\sqrt{L}$ (renormalized energy width). The reason for the rescaling with $\sqrt{L}$ for the width of the LDoS is that in the chaotic regime, the classical width of LDoS can be considered as the sum of L independent random variables S_k^z, whose second moment is proportional to L. With this rescaling, all points collapse onto a single curve well described by a logarithmic fit.

The numerically found logarithmic dependence

$$\tilde{h}_{KS} \propto \ln \tilde{\sigma}_{LDoS}, \tag{24}$$

is a relationship between two intensive quantities. This remarkable result should be checked in other models as well. This is a very important finding, because these two quantities have a completely different dynamical origin. The Kolmogorov-Sinai entropy is directly related to *local* instability, while the LDoS is associated with the *global* properties of the relaxation process. We hope that the relation above will trigger future investigations in the field.

VI. SUMMARY

The aim of our study was to establish the quantum-classical correspondence (QCC) for interacting spin models, which can be strongly chaotic in the classical limit. Our results indicate that this correspondence holds only in the region of strong classical and quantum chaos, which corresponds to the energy region $E \approx 0$, as confirmed from the analysis of the Lyapunov spectrum.

Starting with the analysis of the classical equations of motion, we found that in addition to energy, our model presents other integrals of motion. This property, which is generic to spin systems, stems from the fact that the motion of each individual spin is restricted to a 3D sphere, which results in a many-dimensional phase space with a nonstandard Hamiltonian structure.

We observed that for weak interaction, the motion of each individual spin can be effectively described as a *linear* parametric oscillator under an external force consisting of a large number of harmonics. In this case, one can speak of the emergence of *linear chaos*, a term introduced by Chirikov [105,106].

As the interaction strength increases, the influence of nonlinear resonances emerge due to the nonlinear coupling between the spins. However, our results made it clear that in many aspects the dynamical properties of the model can still be effectively described with the motion of individual spins. In particular, we showed that ergodicity of the full model boils down to ergodicity of the motion of each individual spin. This

allows for the introduction of a test of the *local ergodicity* of the motion of individual spins. Following random matrix theory, ergodic motion of the trajectory on a sphere implies a flat distribution of the components of each spin. Our numerical data confirmed the emergence of this flat distribution for a large enough interaction strength ($J_0 \gtrsim 1$) and sufficiently long spin chains ($L \gg 1$). One can therefore speak of *global ergodicity*, when the motion of *all* spins are *locally ergodic*.

Our study of the quantum counterpart of the system started with the analysis of the structure of the Hamiltonian matrix, which allowed us to establish a criterion for the onset of quantum chaos. We then showed that the shape of the eigenfunctions (SoE) and the local density of states (LDoS), which are essential quantum quantities, have classical analogs that can be obtained using the classical equations of motion. There is an excellent correspondence between the classical and quantum distributions in the region of strong quantum chaos, but not when ergodicity is broken.

In the last section, we presented a compelling relationship between the Kolmogorov-Sinai entropy h_{KS} and the width of the LDoS σ_{LDoS}. Since h_{KS} is related to the local instability of motion, it is not a directly measurable quantity, but σ_{LDoS} is the decay rate of the survival (return) probability, which is a global quantity that can be measured after a quantum quench. This opens the possibility to relate the Kolmogorov-Sinai entropy with a physically measurable quantity.

ACKNOWLEDGMENTS

F.B. acknowledges support by the Iniziativa Specifica INFN-DynSysMath. This work has been financially supported by the Catholic University of Sacred Heart within the program of promotion and diffusion of scientific research. Research has also been financially supported by Ministero dell'Istruzione, dell'Universitá e della Ricerca within the Project No. PRIN 20172H2SC4. F.M.I. acknowledges financial support from CONACyT (Grant No. 286633). L.F.S. had support from the MPS Simons Foundation Award ID 678586. This research was supported by the US National Science Foundation (NSF) Grant No. DMR-1936006. L.B. acknowledges support from UNAM–PAPIIT Grant No. IG-101122.

[1] P. Ehrenfest, Bemerkung über die angenäherte gültigkeit der klassischen mechanik innerhalb der quantenmechanik, Z. Phys. **45**, 455 (1927).
[2] G. Berman and G. Zaslavsky, Condition of stochasticity in quantum nonlinear systems, Physica A **91**, 450 (1978).
[3] B. V. Chirikov, F. M. Izrailev, and D. L. Shepelyansky, Dynamical stochasticity in classical and quantum mechanics, Sov. Sci. Rev. C **2**, 209 (1981).
[4] G. Casati, B. V. Chirikov, F. M. Izrailev, and J. Ford, Stochastic behavior of a quantum pendulum under a periodic perturbation, Lect. Notes in Phys. **93**, 334 (1979).
[5] B. V. Chirikov, F. M. Izrailev, and D. L. Shepelyansky, Quantum chaos: Localization vs. ergodicity, Physica D **33**, 77 (1988).
[6] P. R. Levstein, G. Usaj, and H. M. Pastawski, Attenuation of polarization echoes in nuclear magnetic resonance: A study of the emergence of dynamical irreversibility in many-body quantum systems, J. Chem. Phys. **108**, 2718 (1998).
[7] F. M. Cucchietti, C. H. Lewenkopf, E. R. Mucciolo, H. M. Pastawski, and R. O. Vallejos, Measuring the Lyapunov exponent using quantum mechanics, Phys. Rev. E **65**, 046209 (2002).
[8] D. A. Wisniacki, Short-time decay of the Loschmidt echo, Phys. Rev. E **67**, 016205 (2003).
[9] F. M. Cucchietti, H. M. Pastawski, and R. A. Jalabert, Universality of the Lyapunov regime for the Loschmidt echo, Phys. Rev. B **70**, 035311 (2004).
[10] T. Gorin, T. Prosen, T. H. Seligman, and M. Žnidarič, Dynamics of Loschmidt echoes and fidelity decay, Phys. Rep. **435**, 33 (2006).
[11] A. S. de Wijn, B. Hess, and B. V. Fine, Largest Lyapunov Exponents for Lattices of Interacting Classical Spins, Phys. Rev. Lett. **109**, 034101 (2012).
[12] T. A. Elsayed and B. V. Fine, Sensitivity to small perturbations in systems of large quantum spins, Phys. Scr. **T165**, 014011 (2015).
[13] E. B. Rozenbaum, S. Ganeshan, and V. Galitski, Lyapunov Exponent and Out-of-Time-Ordered Correlator's Growth Rate in a Chaotic System, Phys. Rev. Lett. **118**, 086801 (2017).
[14] A. E. Tarkhov, S. Wimberger, and B. V. Fine, Extracting Lyapunov exponents from the echo dynamics of Bose-Einstein condensates on a lattice, Phys. Rev. A **96**, 023624 (2017).
[15] I. García-Mata, M. Saraceno, R. A. Jalabert, A. J. Roncaglia, and D. A. Wisniacki, Chaos Signatures in the Short and Long Time Behavior of the Out-of-Time Ordered Correlator, Phys. Rev. Lett. **121**, 210601 (2018).
[16] S. Pappalardi, A. Russomanno, B. Žunkovič, F. Iemini, A. Silva, and R. Fazio, Scrambling and entanglement spreading in long-range spin chains, Phys. Rev. B **98**, 134303 (2018).
[17] J. Chávez-Carlos, B. López-del Carpio, M. A. Bastarrachea-Magnani, P. Stránský, S. Lerma-Hernández, L. F. Santos, and J. G. Hirsch, Quantum and Classical Lyapunov Exponents in Atom-Field Interaction Systems, Phys. Rev. Lett. **122**, 024101 (2019).
[18] J. Rammensee, J. D. Urbina, and K. Richter, Many-Body Quantum Interference and the Saturation of Out-of-Time-Order Correlators, Phys. Rev. Lett. **121**, 124101 (2018).
[19] Q. Hummel, B. Geiger, J. D. Urbina, and K. Richter, Reversible Quantum Information Spreading in Many-Body Systems near Criticality, Phys. Rev. Lett. **123**, 160401 (2019).
[20] A. Lakshminarayan, Out-of-time-ordered correlator in the quantum Baker's map and truncated unitary matrices, Phys. Rev. E **99**, 012201 (2019).
[21] S. Pilatowsky-Cameo, J. Chávez-Carlos, M. A. Bastarrachea-Magnani, P. Stránský, S. Lerma-Hernández, L. F. Santos, and J. G. Hirsch, Positive quantum Lyapunov exponents in experimental systems with a regular classical limit, Phys. Rev. E **101**, 010202(R) (2020).
[22] J. Wang, G. Benenti, G. Casati, and W. G. Wang, Complexity of quantum motion and quantum-classical correspondence: A phase-space approach, Phys. Rev. Res. **2**, 043178 (2020).

[23] T. Xu, T. Scaffidi, and X. Cao, Does Scrambling Equal Chaos? Phys. Rev. Lett. **124**, 140602 (2020).

[24] K. Hashimoto, K.-B. Huh, K.-Y. Kim, and R. Watanabe, Exponential growth of out-of-time-order correlator without chaos: Inverted harmonic oscillator, J. High Energ. Phys. 11 (2020) 068.

[25] J. Wang, G. Benenti, G. Casati, and W. G. Wang, Quantum chaos and the correspondence principle, Phys. Rev. E **103**, L030201 (2021).

[26] A. I. Larkin and Yu. N. Ovchinnikov, Quasiclassical method in the theory of superconductivity, Zh. Eksp. Teor. Fiz. **55**, 2262 (1969) [Sov. Phys. JETP **28**, 1200 (1069)].

[27] D. L. Shepelyansky, Some statistical properties of simple classically stochastic quantum systems, Physica D **8**, 208 (1983).

[28] M. V. Berry, Regular and irregular semiclassical wavefunctions, J. Phys. A **10**, 2083 (1977).

[29] V. V. Flambaum, A. A. Gribakina, G. F. Gribakin, and M. G. Kozlov, Structure of compound states in the chaotic spectrum of the Ce atom: Localization properties, matrix elements, and enhancement of weak perturbations, Phys. Rev. A **50**, 267 (1994).

[30] V. Zelevinsky, M. Horoi, and B. Alex Brown, Information entropy, chaos and complexity of the shell model eigenvectors, Phys. Lett. B **350**, 141 (1995).

[31] M. Horoi, V. Zelevinsky, and B. A. Brown, Chaos vs Thermalization in the Nuclear Shell Model, Phys. Rev. Lett. **74**, 5194 (1995).

[32] V. Zelevinsky, B. A. Brown, N. Frazier, and M. Horoi, The nuclear shell model as a testing ground for many-body quantum chaos, Phys. Rep. **276**, 85 (1996).

[33] V. V. Flambaum and F. M. Izrailev, Entropy production and wave packet dynamics in the Fock space of closed chaotic many-body systems, Phys. Rev. E **64**, 036220 (2001).

[34] F. Borgonovi, F. M. Izrailev, L. F. Santos, and V. G. Zelevinsky, Quantum chaos and thermalization in isolated systems of interacting particles, Phys. Rep. **626**, 1 (2016).

[35] G. Casati, F. Valz-Gris, and I. Guarneri, On the connection between quantization of nonintegrable systems and statistical theory of spectra, Lett. Nuov. Cim. **28**, 279 (1980).

[36] O. Bohigas, M. J. Giannoni, and C. Schmit, Characterization of Chaotic Quantum Spectra and Universality of Level Fluctuation Laws, Phys. Rev. Lett. **52**, 1 (1984).

[37] T. Guhr, A. Müller-Groeling, and H. A. Weidenmüller, Random matrix theories in quantum physics: Common concepts, Phys. Rep. **299**, 189 (1998).

[38] F. W. K. Firk and S. J. Miller, Nuclei, primes and the random matrix connection, Symmetry **1**, 64 (2009).

[39] E. P. Wigner, On the statistical distribution of the widths and spacings of nuclear resonance levels, Proc. Cambridge Phil. Soc. **47**, 790 (1951).

[40] C. E. Porter, *Statistical Theories of Spectra: Fluctuations* (Academic Press, New York, 1965).

[41] B. Dietz and F. Haake, Taylor and Padé analysis of the level spacing distributions of random-matrix ensembles, Z. Phys. B **80**, 153 (1990).

[42] M. C. Gutzwiller, *Chaos in Classical and Quantum Mechanics* (Springer, New York, 1990).

[43] G. Casati, B. V. Chirikov, and I. Guarneri, Energy-Level Statistics of Integrable Quantum Systems, Phys. Rev. Lett. **54**, 1350 (1985).

[44] Y. G. Sinai, The absence of the poisson distribution for spacings between quasi-energies in the quantum kicked-rotator model, Physica D **33**, 314 (1988).

[45] Y. G. Sinai, Mathematical problems in the theory of quantum chaos, in *Geometric Aspects of Functional Analysis. Lecture Notes in Mathematics, vol 1469*, edited by L. J. and M. V.D. (Springer, Berlin, 1991).

[46] J. Marklof, *Proceedings of the XIIIth International Congress on Mathematical Physics* (International Press, Boston, 2001) pp. 359–363.

[47] S. Mailoud, F. Borgonovi, and F. M. Izrailev, Spectrum statistics in the integrable Lieb-Liniger model, Phys. Rev. E **104**, 034212 (2021).

[48] H. A. Bethe, On the theory of metal I. eigenvalues and eigenfunctions of a linear chain of atoms, Z. Phys. **71**, 205 (1931).

[49] V. E. Korepin, N. M. Bogoliubov, and A. G. Izergin, *Quantum Inverse Scattering Method and Correlation Functions* (Cambridge University Press, Cambridge, 1993).

[50] L. Benet, F. Leyvraz, and T. H. Seligman, Wigner-Dyson statistics for a class of integrable models, Phys. Rev. E **68**, 045201(R) (2003).

[51] A. Relaño, J. Dukelsky, J. M. G. Gómez, and J. Retamosa, Stringent numerical test of the poisson distribution for finite quantum integrable Hamiltonians, Phys. Rev. E **70**, 026208 (2004).

[52] J. A. Scaramazza, B. S. Shastry, and E. A. Yuzbashyan, Integrable matrix theory: Level statistics, Phys. Rev. E **94**, 032106 (2016).

[53] P. Yu, Z.-Y. Li, H.-Y. Xu, L. Huang, B. Dietz, C. Grebogi, and Y.-C. Lai, Gaussian orthogonal ensemble statistics in graphene billiards with the shape of classically integrable billiards, Phys. Rev. E **94**, 062214 (2016).

[54] J. Wang, G. Benenti, G. Casati, and W. Wang, Statistical and dynamical properties of the quantum triangle map, J. Phys. A **55**, 234002 (2022).

[55] T. Engl, J. Dujardin, A. Argüelles, P. Schlagheck, K. Richter, and J. D. Urbina, Coherent Backscattering in Fock Space: A Signature of Quantum Many-Body Interference in Interacting Bosonic Systems, Phys. Rev. Lett. **112**, 140403 (2014).

[56] D. Waltner, P. Braun, M. Akila, and T. Guhr, Trace formula for interacting spins, J. Phys. A **50**, 085304 (2017).

[57] M. Akila, D. Waltner, B. Gutkin, P. Braun, and T. Guhr, Semiclassical Identification of Periodic Orbits in a Quantum Many-Body System, Phys. Rev. Lett. **118**, 164101 (2017).

[58] M. Akila, B. Gutkin, P. Braun, D. Waltner, and T. Guhr, Semiclassical prediction of large spectral fluctuations in interacting kicked spin chains, Ann. Phys. **389**, 250 (2018).

[59] A. Chan, A. De Luca, and J. T. Chalker, Solution of a Minimal Model for Many-Body Quantum Chaos, Phys. Rev. X **8**, 041019 (2018).

[60] B. Pozsgay, Algebraic Construction of Current Operators in Integrable Spin Chains, Phys. Rev. Lett. **125**, 070602 (2020).

[61] D. Schubert, J. Richter, F. Jin, K. Michielsen, H. D. Raedt, and R. Steinigeweg, Quantum versus classical dynamics in spin models: Chains, ladders, and square lattices, Phys. Rev. B **104**, 054415 (2021).

[62] V. V. Flambaum and F. M. Izrailev, Statistical theory of finite Fermi systems based on the structure of chaotic eigenstates, Phys. Rev. E **56**, 5144 (1997).

[63] F. Borgonovi, F. Mattiotti, and F. M. L. F. Izrailev, Temperature of a single chaotic eigenstate, Phys. Rev. E **95**, 042135 (2017).

[64] F. Borgonovi, F. M. Izrailev, and L. F. Santos, Exponentially fast dynamics of chaotic many-body systems, Phys. Rev. E **99**, 010101(R) (2019).

[65] P. Richerme, Z.-X. Gong, A. Lee, C. Senko, J. Smith, M. Foss-Feig, S. Michalakis, A. V. Gorshkov, and C. Monroe, Non-local propagation of correlations in quantum systems with long-range interactions, Nature (London) **511**, 198 (2014).

[66] P. Jurcevic, B. P. Lanyon, P. Hauke, C. Hempel, P. Zoller, R. Blatt, and C. F. Roos, Quasiparticle engineering and entanglement propagation in a quantum many-body system, Nature (London) **511**, 202 (2014).

[67] J. Smith, A. Lee, P. Richerme, B. Neyenhuis, P. W. Hess, P. Hauke, M. Heyl, D. A. Huse, and C. Monroe, Many-body localization in a quantum simulator with programmable random disorder, Nat. Phys. **12**, 907 (2016).

[68] T. Brydges, A. Elben, P. Jurcevic, B. Vermersch, C. Maier, B. P. Lanyon, P. Zoller, R. Blatt, and C. F. Roos, Probing Rényi entanglement entropy via randomized measurements, Science **364**, 260 (2019).

[69] F. Borgonovi, I. Guarneri, and F. M. Izrailev, Quantum-classical correspondence in energy space: Two interacting spin-particles, Phys. Rev. E **57**, 5291 (1998).

[70] F. M. Izrailev, Quantum-classical correspondence for isolated systems of interacting particles: Localization and ergodicity in energy space, Phys. Scr. **T90**, 95 (2001).

[71] F. Borgonovi, I. Guarnieri, F. M. Izrailev, and G. Casati, Chaos and thermalization in a dynamical model of two interacting particles, Phys. Lett. A **247**, 140 (1998).

[72] G. A. Luna-Acosta, J. A. Mendez-Bermudez, and F. M. Izrailev, Periodic chaotic billiards: Quantum-classical correspondence in energy space, Phys. Rev. E **64**, 036206 (2001).

[73] G. A. Luna-Acosta, J. A. Mendez-Bermudez, and F. Izrailev, Chaotic electron motion in superlattices. Quantum-classical correspondence of the structure of eigenstates and ldos, Phys. E **12**, 267 (2002).

[74] L. Benet, F. Izrailev, T. Seligman, and A. Suarez Moreno, Semiclassical properties of eigenfunctions and occupation number distribution for a model of two interacting particles, Phys. Lett. A **277**, 87 (2000).

[75] L. Benet, J. Flores, H. Hernandez-Salgana, F. Izrailev, F. Levyraz, and T. Seligman, Fluctuations of wave functions about their classical average, J. Phys. A: Math. Gen. **36**, 1289 (2003).

[76] M. Rautenberg and M. Gärttner, Classical and quantum chaos in a three-mode bosonic system, Phys. Rev. A **101**, 053604 (2020).

[77] G. M. Zaslavsky, *Hamiltonian Chaos and Fractional Dynamics* (Oxford University Press, Oxford, 2005).

[78] P. A. Miller and S. Sarkar, Signatures of chaos in the entanglement of two coupled quantum kicked tops, Phys. Rev. E **60**, 1542 (1999).

[79] C. T. Asplund and D. Berenstein, Entanglement entropy converges to classical entropy around periodic orbits, Ann. Phys. **366**, 113 (2016).

[80] E. Bianchi, L. Hackl, and N. Yokomizo, Linear growth of the entanglement entropy and the Kolmogorov-Sinai rate, J. High Energy Phys. 03 (2018) 025.

[81] F. Borgonovi, F. M. Izrailev, and L. F. Santos, Timescales in the quench dynamics of many-body quantum systems: Participation ratio versus out-of-time ordered correlator, Phys. Rev. E **99**, 052143 (2019).

[82] B. V. Chirikov, Resonance processes in magnetic traps, Sov. J. At. Energy **6**, 464 (1960).

[83] B. V. Chirikov, Resonance processes in magnetic traps, J. Nucl. Energy. Part C Plasma Phys. **1**, 253 (1960).

[84] F. Izrailev, Nearly linear mappings and their applications, Physica D **1**, 243 (1980).

[85] S. Iubini and A. Politi, Chaos and localization in the discrete nonlinear Schrödinger equation, Chaos, Solitons and Fractals **147**, 110954 (2021).

[86] C. Skokos, The Lyapunov characteristic exponents and their computation, *Dynamics of Small Solar System Bodies and Exoplanets* (Springer, Berlin, 2009) pp. 63–135.

[87] A. Pikovsky and A. Politi, *Lyapunov Exponents* (Cambridge University Press, Cambridge, 2016).

[88] Y. B. Pesin, Characteristic Lyapunov exponents and smooth ergodic theory, Russian Math. Surveys **32**, 55 (1977).

[89] G. M. Zaslavsky, Stochasticity in quantum systems, Phys. Rep. **80**, 157 (1981).

[90] T. A. Brody, J. Flores, J. B. French, P. A. Mello, A. Pandey, and S. S. M. Wong, Random-matrix physics: Spectrum and strength fluctuations, Rev. Mod. Phys. **53**, 385 (1981).

[91] F. M. Izrailev, Simple models of quantum chaos: Spectrum and eigenfunctions, Phys. Rep. **196**, 299 (1990).

[92] G. P. Berman, F. Borgonovi, F. M. Izrailev, and V. I. Tsifrinovich, Delocalization border and onset of chaos in a model of quantum computation, Phys. Rev. E **64**, 056226 (2001).

[93] L. F. Santos and M. Rigol, Onset of quantum chaos in one-dimensional bosonic and fermionic systems and its relation to thermalization, Phys. Rev. E **81**, 036206 (2010).

[94] E. J. Torres-Herrera and L. F. Santos, Local quenches with global effects in interacting quantum systems, Phys. Rev. E **89**, 062110 (2014).

[95] L. F. Santos, F. Pérez-Bernal, and E. J. Torres-Herrera, Speck of chaos, Phys. Rev. Res. **2**, 043034 (2020).

[96] F. Haake, *Quantum Signatures of Chaos* (Springer-Verlag, Berlin, 1991).

[97] L. A. Khalfin, Zh. Eksp. Teor. Fiz. **33**, 1371 (1958) [Sov. Phys. JETP **6**, 1053 (1958)].

[98] G. N. Fleming, A unitarity bound on the evolution of nonstationary states, Il Nuovo Cim. **16**, 232 (1973).

[99] V. V. Flambaum, Time dynamics in chaotic many-body systems: Can chaos destroy a quantum computer? Aust. J. Phys. **53**, 489 (2000).

[100] V. V. Flambaum and F. M. Izrailev, Unconventional decay law for excited states in closed many-body systems, Phys. Rev. E **64**, 026124 (2001).

[101] E. J. Torres-Herrera, J. Karp, M. Távora, and L. F. Santos, Realistic many-body quantum systems vs. full random matrices: Static and dynamical properties, Entropy **18**, 359 (2016).

[102] M. Schiulaz, E. J. Torres-Herrera, and L. F. Santos, Thouless and relaxation time scales in many-body quantum systems, Phys. Rev. B **99**, 174313 (2019).

[103] G. Casati, B. V. Chirikov, I. Guarneri, and F. M. Izrailev, Band-random-matrix model for quantum localization in conservative systems, Phys. Rev. E **48**, R1613 (1993).

[104] G. Casati, B. V. Chirikov, I. Guarneri, and F. M. Izrailev, Quantum ergodicity and localization in conservative systems: The Wigner band random matrix model, Phys. Lett. A **223**, 430 (1996).

[105] B. V. Chirikov, Linear chaos, in *Nonlinearity with Disorder*, Proceedings in Physics No. 67, edited by S. P. F. Abdulaev and A. R. Bishop (Springer, Berlin, 1992), p. 3.

[106] B. Chirikov, Linear and nonlinear dynamical chaos, Open Syst. Inf. Dyn. **4**, 241 (1997).